Journal of Inorganic Biochemistry 191 (2019) 126–134

Contents lists available at ScienceDirect

Journal of Inorganic Biochemistry

journal homepage: www.elsevier.com/locate/jinorgbio

A ruthenium(II) complex containing a *p*-cresol group induces apoptosis in human cervical carcinoma cells through endoplasmic reticulum stress and reactive oxygen species production

Li Xu[a,*], Pei-Pei Zhang[a], Xiao-Qiang Fang[a], Yan Liu[a], Jin-Quan Wang[b], Hui-Zhuo Zhou[a], Shu-Ting Chen[a], Hui Chao[c,*]

[a] School of Chemistry and Chemical Engineering, Guangdong Pharmaceutical University, Zhongshan, 528458, PR China
[b] School of Bioscience and Biopharmaceutics, Guangdong Province Key Laboratory for Biotechnology Drug Candidates, Guangdong Pharmaceutical University, Guangzhou, 510006, PR China
[c] MOE Key Laboratory of Bioinorganic and Synthetic Chemistry, School of Chemistry and Chemical Engineering, Sun Yat-Sen University, Guangzhou 510275, PR China

ARTICLE INFO

Keywords:
Ruthenium (II) complexes
Apoptosis
Cytotoxicity
Endoplasmic reticulum stress

ABSTRACT

The chemical structures of Ru (II) complexes are known to affect their cellular behavior and toxicity. In this study, three new luminescent Ru (II) complexes, $[Ru(bpy)_2(\mathbf{HIPMP})](ClO_4)_2$ (**Ru1**, bpy = 2,2′-bipyridine, **HIPMP** = 2-(1*H*-imidazo-[4,5-f] [1,10] phenanthrolin-2-yl)-4-methylphenol), $[Ru(phen)_2(\mathbf{HIPMP})](ClO_4)_2$ (**Ru2**, phen = 1,10-phenanthroline), $[Ru(dmb)_2(\mathbf{HIPMP})](ClO_4)_2$ (**Ru3**, dmb = 4,4′-dimethyl-2,2′-bipyridine), were synthesized, and their anticancer activities were examined. All three complexes displayed anticancer activities against various cancer cells, with **Ru2** exhibiting the highest cytotoxic activities. **Ru2** was shown to accumulate specifically in the endoplasmic reticulum (ER) and induce ER stress-mediated apoptosis. In addition, **Ru2** could generate reactive oxygen species (ROS) and trigger mitochondrial membrane potential depolarization. These results demonstrated that **Ru2** induced apoptosis in HeLa cells through ER stress and ROS production.

1. Introduction

Based on their unique and versatile biochemical properties, ruthenium-based complexes have been regarded as promising anticancer agents for alternative drugs to cisplatin and its derivatives [1]. The first two approved Ru(III) complexes, namely, NAMI-A(H_2Im)[*trans*-$RuCl_4$(DMSO)(HIm)], where HIm = 1*H*-imidazole and DMSO = dimethylsulfoxide) [2] and KP1019 (H_2Ind)[*trans*-$RuCl_4$(HInd)$_2$], where Hind = 1*H*-indazole) [3], have successfully been used in clinical studies. Recently, many ruthenium (II) complexes with potent therapeutic properties have been designed and developed as anticancer drugs, including inorganic Ru (II), organometallic Ru (II) and nanomaterial Ru (II) complexes [4–7]. Furthermore, several mechanisms have been applied to elucidate the anticancer activities of Ru (II) complexes depending on their intracellular targets, which include nucleic acids [8], proteins [9,10], and cell organelles [11,12]. A different pathway of cell apoptosis involving endoplasmic reticulum (ER) stress induced by metal complexes, such as ruthenium- [13,14], iridium- [15–17], platinum- [18,19] and lanthanide-based complexes [20] has been reported.

The ER is a cytoplasmic organelle for the folding and trafficking of secretory and membrane proteins [21] as well as intracellular calcium storage, making it very important in cellular signal-transducing [22] and extremely sensitive to alterations in homeostasis and to a number of biochemical and physiological stimuli. The perturbation of ER functions leads to ER stress, such as the accumulation of unfolded or misfolded proteins [23] and the failure of the ER to cope with an excessive protein load. ER stress causes an imbalance between ER protein folding load and capacity. Severe ER stress can activate intrinsic apoptosis, resulting in cell death. Certain cancer cells, including multiple myelomacells, possessing high ER activity are especially sensitive to ER stress-mediated cell death [24]. Thus, the development of anticancer drugs that affect ER stress-mediated apoptosis pathways could be an effective therapeutic strategy [25].

ROS are thought to play important roles in the induction of apoptosis by Ru (II) complexes in cancer cells [26–28]. ROS have been proven to cause cellular damage, such as damaging lipids, proteins and DNA in early stages of apoptosis [29]. Additionally, ROS trigger the depolarization of the mitochondrial membrane and induce

* Corresponding authors.
E-mail addresses: xuli473@163.com (L. Xu), ceschh@mail.sysu.edu.cn (H. Chao).

https://doi.org/10.1016/j.jinorgbio.2018.11.015
Received 28 July 2018; Received in revised form 21 November 2018; Accepted 25 November 2018
Available online 28 November 2018
0162-0134/

mitochondrial dysfunction [30].

In this study, we synthesized and characterized three new Ru(II) complexes $[Ru(N{-}N)_2(HIPMP)](ClO_4)_2$ (N-*N* = 2,2′-bipyridine (bpy, **Ru1**), 1,10-phenanthroline (phen, **Ru2**), and 4,4′-dimethyl-2,2′-bipyridine (dmb, **Ru3**). **Ru2** showed higher cytotoxicity than **Ru1** and **Ru3**. Further investigations indicated that **Ru2** can induce ER stress and ROS-mediated mitochondrial dysfunction in the apoptotic signaling pathway, indicating that **Ru2** has the potential to serve as an emerging chemotherapeutic agent for cancer therapy.

2. Experimental section

2.1. Materials

All reagents and solvents were purchased commercially and used without further purification unless specifically noted. Cisplatin, propidium iodide (PI), 3-(4,5-dimethylthiazol-2-yl)-2,5-diphenyl-tetrazoliumbromide (MTT), dimethyl sulfoxide(DMSO), $RuCl_3{\cdot}xH_2O$, 2,2′-bipyridine (bpy), 1,10-phenanthroline, 4,4′-dimethyl-2,2′-bipyridine and 2-hydroxy-5-methylbenzaldehyde were obtained from Sigma Aldrich. Lyso Tracker Green DND-26 (LTG), MitoTracker Green FM (MTG), ER-Tracker™ Green, and 5,5′,6,6′-tetrachloro-1,1′,3,3′-tetraethylbenzimidazolylcarbocyanine iodide (JC-1) were obtained from Life Technologies (USA). Stock solutions of cisplatin (10 mM) and ruthenium (II) complexes (1 mM) were prepared in DMSO and were stable for at least 48 h at room temperature, as monitored by UV–visible spectroscopy. Doubly distilled water was used in all experiments.

2.2. Physical measurements

Microanalysis (C, H, and N) was performed by a Perkin-Elmer 240Q elemental analyzer. Fast atom bombardment (FAB) mass spectra were recorded on a VG ZAB-HS spectrometer in a 3-nitrobenzylalcohol matrix. Electrospray ionization mass spectrometry (ES-MS) was carried out on an LCQ system (Finnigan MAT, USA) using methanol as the mobile phase. The spray voltage, tube lens offset, capillary voltage and capillary temperature were set at 4.50 kV, 30.00 V, 23.00 V and 200 °C, respectively, and the quoted *m/z* values are for the major peaks in the isotope distribution. ^{1}HNMR spectra were acquired at room temperature on a Bruker AVANCE AV 400 NMR spectrometer with DMSO-d_6 as the solvent and tetramethylsilane (TMS) as an internal standard.

2.2.1. Synthesis of the ligand and complexes

2.2.1.1. Synthesis of 2-(1H-imidazo-[4,5-f][1,10] phenanthrolin-2-yl)-4-methylphenol (HIPMP). 2-Hydroxy-5-methylbenzaldehyde (0.20 g, 1.5 mmol), 1,10-phenanthroline-5,6-dione (0.32 g, 1.5 mmol) [31], and ammonium acetate (2.31 g, 30 mmol) were placed in a round-bottom flask, dissolved in 30 mL of glacial acetic acid, and refluxed for 4 h. After cooling, precipitate was obtained upon dropwise addition of concentrated aqueous ammonia. The precipitate was purified by column chromatography on a silica gel column (60–100 mesh) with ethanol as the eluent. Yield: 0.39 g, 80%. Anal.Calcd for $C_{20}H_{14}N_4O$: C, 73.61; H, 4.32; N, 17.17. Found: C, 73.29; H, 4.64; N, 17.39%. FAB-MS: *m/z* = 327(M + 1).

2.2.1.2. Synthesis of $[Ru(bpy)_2(HIPMP)](ClO_4)_2$ (Ru1). A mixture containing *cis*-$[Ru(bpy)_2Cl_2]{\cdot}2H_2O$ (0.26 g, 0.5 mmol) [32] and **HIPMP** (0.16 g, 0.5 mmol) in ethanol (60 cm^3) was heated to reflux under argon for 8 h to give a clear red solution. Upon cooling, a saturated aqueous $NaClO_4$ solution was added. The red precipitate was filtered, washed with water and diethyl ether, and dried *in vacuo*. The crude product was purified by column chromatography on neutral alumina eluted with methyl cyanide (MeCN)-ethanol (10:1, v/v). The red band was collected, the solvent was evaporated until it was dry under reduced pressure, and then, red powder was obtained. Yield: 0.33 g, 70%. Anal. Calcd for $C_{40}H_{30}N_8Cl_2O_9Ru$: C, 51.18; H, 3.22; N, 11.94%; Found: C, 50.78; H, 3.34; N, 12.08%. ES-MS [CH_3CN, *m/z*]: 739.2 ($[M{-}2ClO_4{-}H]^+$), 370.1 ($[M{-}2ClO_4]^{2+}$). ^{1}HNMR (400 MHz, DMSO-d_6): δ 13.02 (s, 1H), 10.82 (s, 1H), 9.08 (d, 2H, *J* = 8.5 Hz), 8.88 (d, 2H, *J* = 9.0 Hz), 8.84 (d, 2H, *J* = 8.0 Hz), 8.22 (d, 2H, *J* = 8.2 Hz), 8.12 (d, 2H, *J* = 7.8 Hz), 8.09 (d, 2H, *J* = 6.5 Hz), 7.98 (d, 2H, *J* = 7.6 Hz), 7.87 (t, 3H, *J* = 6.5 Hz), 7.61 (d, 2H, *J* = 8.0 Hz), 7.59 (d, 2H, *J* = 7.6 Hz), 7.36 (t, 2H, *J* = 6.5 Hz), 7.16 (d, 1H, *J* = 7.6 Hz), 6.93 (d, 1H, *J* = 7.6 Hz), 2.48 (s, 3H).

2.2.1.3. Synthesis of $[Ru(phen)_2(HIPMP)](ClO_4)_2$ (Ru2). This complex was obtained according to an identical method as described for **Ru1** by using *cis*-$[Ru(phen)_2Cl_2]{\cdot}2H_2O$ [32] in place of *cis*-$[Ru(bpy)_2Cl_2]{\cdot}2H_2O$. Yield: 0.32 g, 65%. Anal. Calcd for $C_{44}H_{30}N_8Cl_2O_9Ru$: C, 53.56; H, 3.06; N, 11.36%; Found: C, 53.23; H, 3.24; N, 11.69%. ES-MS [CH_3CN, *m/z*]: 787.2 ($[M{-}2ClO_4{-}H]^+$), 394.1 ($[M{-}2ClO_4]^{2+}$). ^{1}HNMR (400 MHz, DMSO-d_6): δ 9.18 (d, 1H, *J* = 8.5 Hz), 9.03 (d, 1H, *J* = 8.0 Hz), 8.76 (m, 4H), 8.39 (d, 4H, *J* = 7.6 Hz), 8.12 (m, 6H), 7.84 (m, 2H), 7.76 (m, 4H), 7.66 (m, 1H), 7.39 (dd, 1H, *J* = 7.8, 8.0 Hz), 7.12 (d, 1H, *J* = 8.2 Hz), 7.04 (s, 1H), 6.85 (d, 1H, *J* = 8.0 Hz), 2.53 (s, 3H).

2.2.1.4. Synthesis of $[Ru(dmb)_2(HIPMP)](ClO_4)_2$ (Ru3). This complex was prepared in a manner identical to that described for **Ru1 by** using *cis*-$[Ru(dmb)_2Cl_2]{\cdot}2H_2O$ [32] in place of *cis*-$[Ru(bpy)_2Cl_2]{\cdot}2H_2O$. Yield: 0.34 g, 68%. $C_{44}H_{38}N_8Cl_2O_9Ru$: C, 53.12; H, 3.85; N, 11.26%; Found: C, 53.52; H, 3.51; N, 11.01%. ES-MS [CH_3CN, *m/z*]: 795.2 ($[M{-}2ClO_4{-}H]^+$), 398.1 ($[M{-}2ClO_4]^{2+}$). ^{1}HNMR (400 MHz, DMSO-d_6): δ 9.18 (d, 1H, *J* = 7.6 Hz), 9.02 (d, 1H, *J* = 7.6 Hz), 8.94 (d, 1H, *J* = 8.0 Hz), 8.72 (d, 1H, *J* = 7.6 Hz), 8.68 (d, 1H, *J* = 7.6 Hz), 8.19 (m, 1H), 8.12 (d, 1H, *J* = 6.5 Hz), 8.04 (d, 1H, *J* = 8.0 Hz), 7.96 (m, 1H), 7.86 (d, 2H, *J* = 8.0 Hz), 7.76 (dd, 2H, *J* = 7.6, 7.8 Hz), 7.68 (d, 2H, *J* = 8.0 Hz), 7.64 (d, 1H, *J* = 8.5 Hz), 7.39 (m, 2H), 7.15 (d, 2H, *J* = 8.0 Hz), 7.10 (d, 1H, *J* = 8.5 Hz), 7.01 (d, 1H, *J* = 7.6 Hz), 6.83 (d, 1H, *J* = 7.6 Hz), 2.61 (s, 12H), 2.50 (s, 3H).

2.2.2. Cell lines and cell culture

The hepatocellular carcinoma cell line HepG2, the cervical carcinoma cell line HeLa, the nasopharyngeal carcinoma cell line CNE-1 and the human lung carcinoma cell line A549 were obtained from the Experimental Animal Center of Sun Yat-Sen University (Guangzhou, China). L02 normal hepatic cells were obtained from the cell bank of the Cell Institute of Sinica Academia Shanghai (Shanghai, China). All cell lines were incubated in 25 cm^2 culture flasks in either Roswell Park Memorial Institute 1640 (RPMI-1640, Invitrogen, Carlsbad, CA) or Dulbecco's modified Eagle's medium (DMEM, Gibco, Gaithersburg, MD) containing 10% fetal bovine serum (FBS), 100 units mL^{-1} penicillin and 50 units mL^{-1} streptomycin at 37 °C in a humidified atmosphere with 5% CO_2. The cells were cultured until they reached the logarithmic growth phase unless otherwise specified.

2.2.3. Cytotoxicity assay in vitro

Cell cytotoxicity upon treatment with Ru (II) complexes was evaluated using the MTT assay [33]. Cells were cultured in 96-well microassay culture plates (2×10^4 cells per well) and incubated in 5% CO_2 at 37 °C overnight. The cells were treated with the tested complexes, control wells were prepared by the addition of culture medium (100 μL), and cisplatin was included as a positive control agent. The plates were incubated at 37 °C in a 5% CO_2 incubator for 48 h. After incubation, MTT solution (MTT working solution, 5 mg mL^{-1} phosphate-buffered saline, 20 μL/well) was added, and the cells were incubated for 4 h. Then, the medium was removed, and 150 μL/well of isopropanol was added to dissolve the formazan. The absorbance (λ = 570 nm) was measured on a microplate reader. The IC_{50} value was determined by the plots of viability *versus* the dose used to treat the cells. Error bars were calculated as the standard error of three independent experiments.

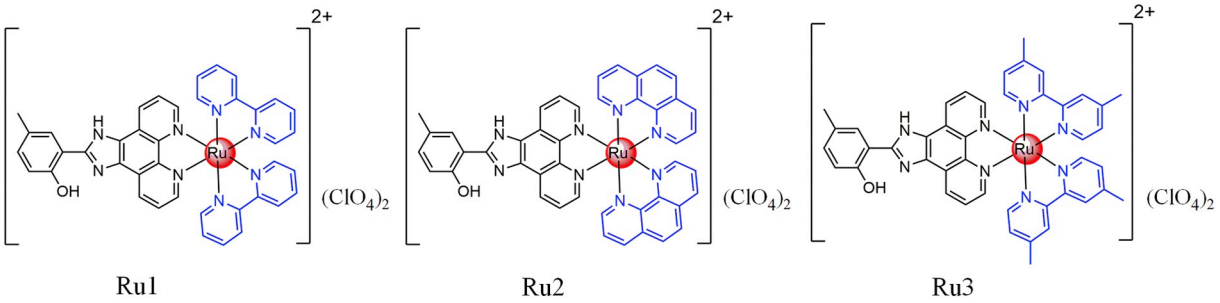

Scheme 1. Chemical structures of ruthenium (II) complexes **Ru1**, **Ru2** and **Ru3**.

2.2.4. Cellular localization analysis

HeLa cells were plated on a 35 mm cell culture dish (Corning) at a density of 2×10^4 cells per dish. After incubation for one day at 37 °C under 5% CO_2, the cells were washed with phosphate-buffered saline (PBS) and then treated with or without 20.0 μM **Ru2** in PBS (pH = 7.4) for 1 h at 37 °C. After washing the cells with PBS buffer three times to remove the remaining **Ru2**, the HeLa cells were further incubated with ER-Tracker™ (1 μM), LysoTracker® (100 nM), MitoTracker® (50 nM) and 4′,6-diamino-2-phenylindole (DAPI) (5 μg mL^{-1}) for 30 min. The cells were carefully washed three times with PBS buffer and then observed under an inverted fluorescence microscope (Olympus IX71) or a confocal microscope (Zeiss LSM 710 NLO, 63×/NA 1.4 oil immersion objective).

2.2.5. Inductively Coupled Plasma Mass Spectrometry (ICP-MS) Analysis

The ruthenium content in different subcellular compartments was measured using an Agilent ICP-MS, as described in our previous report [27]. HeLa cells were plated into 100 mm tissue culture plates (Costar) and **Ru2** (final concentration 10.0 μM) was added to the culture medium for 24 h. The cytoplasmic and nuclear fractions were separated using a nucleus extraction Kit (Pierce, Thermo) following the manufacturer's protocol. The mitochondrial fractions were extracted using a mitochondrial extraction Kit (Pierce, Thermo). The results were reported as picograms of ruthenium per cell. The data were reported as the mean ± standard deviation ($n = 3$).

2.2.6. Annexin V/PI double staining

HeLa cells (1×10^6) were plated in each well of a 6-well plate and treated with **Ru2** at different concentrations (10, 20, 40 μM) for 24 h. Cells were trypsinized, washed twice with ice-cold PBS and then stained with 5 μL of Alexa Fluor 488 annexin V stock (Invitrogen, Paisley, UK) and 1 μL of PI (1 mg mL^{-1}, Sigma, USA) in 100 μL of binding buffer (50 mmolL^{-1} HEPES/NaOH, pH 7.4, 700 mmol L^{-1} NaCl, 12.5 mmol L^{-1} $CaCl_2$) for 15 min at room temperature in the dark. Another 400 μL of binding buffer was added, and the apoptotic cells were evaluated by flow cytometry on a FACSCanto II (BD Biosciences, USA).

2.2.7. Transient transfection of siRNA

RNA interference was used to silence CHOP gene expression. Specific and non-specific control siRNAs (Geneseed Biotech Ltd., China) were transfected into cells using Lipofectamine™ 2000 (Invitrogen, USA) according to the manufacture's protocol. The sequence of the siRNA for CHOP was: sense, 5′GGCUCAAGCAGGAAAUCGA; antisense, 5′UCGAUUUCCUGCUUGAGCC. The irrelevant scrambled RNA served as a control.

In briefly, each siRNA and Lipofectamine™ 2000 was respectively diluted in the appropriate amount of medium (Invitrogen, USA) without serum. After 5 min incubation, the diluted siRNA was combined with the diluted Lipofectamine™ 2000 and incubated for 20 min at room temperature. The siRNA-Lipofectamine™ 2000 complexes were added to each well containing cells at 40–60% confluency and cells were incubated at 37 °C in a CO_2 incubator for 24 h. Then cells were incubated at 37 °C for a further 48 h subjected to **Ru2** at indicated concentrations. The cells were then collected for verification of CHOP knockdown by real-time polymerase chain reaction (RT-PCR) (S1) and western blot, and for analyses of cell viability.

2.2.8. Western-blot analysis

After treatment with 10, 20 and 40 μM **Ru2**, exponentially growing HeLa cells were washed with ice-cold PBS twice and lysed in radioimmunoprecipitation assay (RIPA) buffer (150 mM NaCl, 1% NP-40, 0.1% sodium dodecyl sulfate (SDS), 1 mM phenylmethanesulfonyl fluoride (PMSF), 0.5% sodium deoxycholate, 2 mg mL^{-1} aprotinin, 100 mM leupeptin, and 50 mM tris(hydroxymethyl)aminomethane (Tris)-HCl, pH 8.0) to extract the total cellular proteins. Equal amounts of proteins (20–50 μg) were fractionated by SDS-polyacrylamide gel electrophoresis (SDS-PAGE) and then transferred onto polyvinylidene difluoride (PVDF) membranes (Millipore, MA, USA). The membranes were blocked with 5% nonfat dried milk in TBST buffer (50 mM Tris, 150 mM NaCl and 0.1% Tween-20, pH 7.6) and then hybridized with the respective primary antibodies (Santa Cruz Biotechnology, Santa Cruz, CA) overnight. Further incubation with the appropriate horseradish peroxidase-conjugated secondary antibodies was performed. The protein expression levels were visualized using an enhanced chemiluminescence (ECL) detection kit (Pierce Biotechnology, Rockford, IL).

2.2.9. ROS measurement

HeLa cells were incubated with **Ru2** or H_2O_2 at different concentrations for 12 h, and untreated cells were used as a control. Then, the cells were treated with 10 μM 2,7-dichlorodihydrofluorescein diacetate (DCFH-DA) for 30 min at 37 °C. The cells were washed twice with PBS, followed by examination of the intracellular ROS levels through flow cytometry (FACSCanto II, BD Biosciences, USA) and a microplate analyzer (Infinite M200, Tecan, Männedorf, Switzerland). *N*-acetylcysteine (NAC;10 mM) was applied 1 h before the treatment with **Ru2** or H_2O_2 and was kept in the medium during treatment until the cells

Table 1
The IC_{50} values of tested complexes toward different cell lines.

Complex	IC_{50} (μM)				
	HeLa	HepG2	A-549	CNE-1	LO2
Ru1	29.3 ± 3.4	32.4 ± 3.6	36.5 ± 3.4	38.8 ± 5.6	128 ± 3.6
Ru2	18.1 ± 2.8	28.2 ± 5.2	29.8 ± 4.2	31.2 ± 3.6	100.6 ± 0.4
Ru3	39.8 ± 4.1	42.1 ± 4.6	46.8 ± 5.6	48.5 ± 5.7	135.8 ± 6.2
Cisplatin	20.8 ± 3.2	31.2 ± 2.8	28.5 ± 4.2	30.5 ± 2.6	14.3 ± 0.2

were analyzed. Data acquisition and analysis of the flow cytometry data were performed using FlowJo software.

2.2.10. Mitochondrial membrane potential assay

A quantity of 1.5×10^4 HeLa cells was seeded in six-well plates. **Ru2** at various concentrations (10, 20 and 40 μM) were added to the cells for 12 h. A control well was kept without treatment with any complex. Cells were then washed twice with PBS (pH 7.4) and incubated with 5 mg mL^{-1} JC-1 dye at 37 °C for 30 min. The stained cells were observed and analyzed using an inverted fluorescence microscope.

2.3. Statistical analysis

All biological experiments were carried out at least twice with triplicates in each experiment, and representative results were depicted in this report and data were presented as the means ± standard deviations.

3. Results and discussion

3.1. Synthesis and characterization

The structures of **Ru1**, **Ru2** and **Ru3** are illustrated in Scheme 1. The ligand **HIPMP** was obtained in good yield by reacting 1,10-phenanthroline-5,6-dione with 2-hydroxy-5-methylbenzaldehyde by refluxing glacial acetic acid containing ammonium acetate at a molar ratio of 1:1. **HIPMP** was used as the starting material in a reaction with the appropriate molar ratios of the precursor complexes in ethanol, resulting in relatively high yields for **Ru1–Ru3**. The desired Ru(II) complexes were purified using column chromatography on neutral alumina and characterized *via* ^{1}H NMR spectroscopy, elemental analysis, and ES-MS (Fig. S1–S6).

3.2. Cytotoxicity assays in vitro

We evaluated the *in vitro* cytotoxic activities of **Ru1**, **Ru2** and **Ru3** on four selected human cancer cell lines (HeLa, HepG2, A-549, CNE-1) and one normal cell line (L02) using the MTT method to determine potential of these complexes as anticancer agents. Cisplatin was included as a positive control. The above cell lines were incubated with different concentrations of **Ru1**, **Ru2** and **Ru3** for 48 h, and the IC_{50} values for **Ru1**, **Ru2** and **Ru3** against these cell lines are presented in Table 1. The four compounds exhibited *in vitro* antiproliferative activity in the following descending order: **Ru2** > cisplatin > **Ru1** > **Ru3**. Notably, the IC_{50} values of **Ru2** were lower than those of **Ru1** and **Ru3**, indicating that **Ru2** had a higher cytotoxicity than **Ru1** and **Ru3**. Based on the results, we speculate that there is a good correlation between the antitumor activity of the complex and its specific molecular structure. Additionally, some reports have indicated that variation in the ancillary ligands of the Ru(II) complexes may cause some difference in the biological activities of the complexes [34,35]. **Ru1–Ru3**, especially **Ru2**, exhibited potent toxicity against tumor cells and were less toxic to the normal human liver cell line L02 than cisplatin, suggesting that **Ru2** showed high selectivity between tumor cells and normal cells. **Ru2** had the highest sensitivity to HeLa cells, thus, this cell line was selected to investigate the anticancer activity and mechanism studies.

3.3. Subcellular distribution

We subsequently examined the subcellular localization of **Ru2** by fluorescence microscopy. HeLa cells were incubated with 20 μM **Ru2** for only 30 min, resulting in a time-dependent increase in the Ru levels in the cytoplasm. The cellular distribution of **Ru2** was observed by staining the organelles with specific fluorescent probes. As shown in Fig. 1, a high degree of overlap, indicated by the yellow color, between the signals for **Ru2** (red) and ER-Tracker™ (green) was observed. Meanwhile, little superimposition between lysosome-specific Lysotracker® (green), mitochondria-specific Mitotracker® (green) and **Ru2** was detected, respectively. We further performed confocal luminescence imaging experiments to confirm the specific subcellular location by using **Ru2**, ER-Tracker™ and DAPI dyes (Fig. 2) to co-label HeLa cells. As shown in Fig. 2, the confocal images of **Ru2** were almost completely overlaid with those of the commercial ER dye ER-Tracker™. The Pearson's colocalization coefficient of **Ru2** with ER-Trackert was

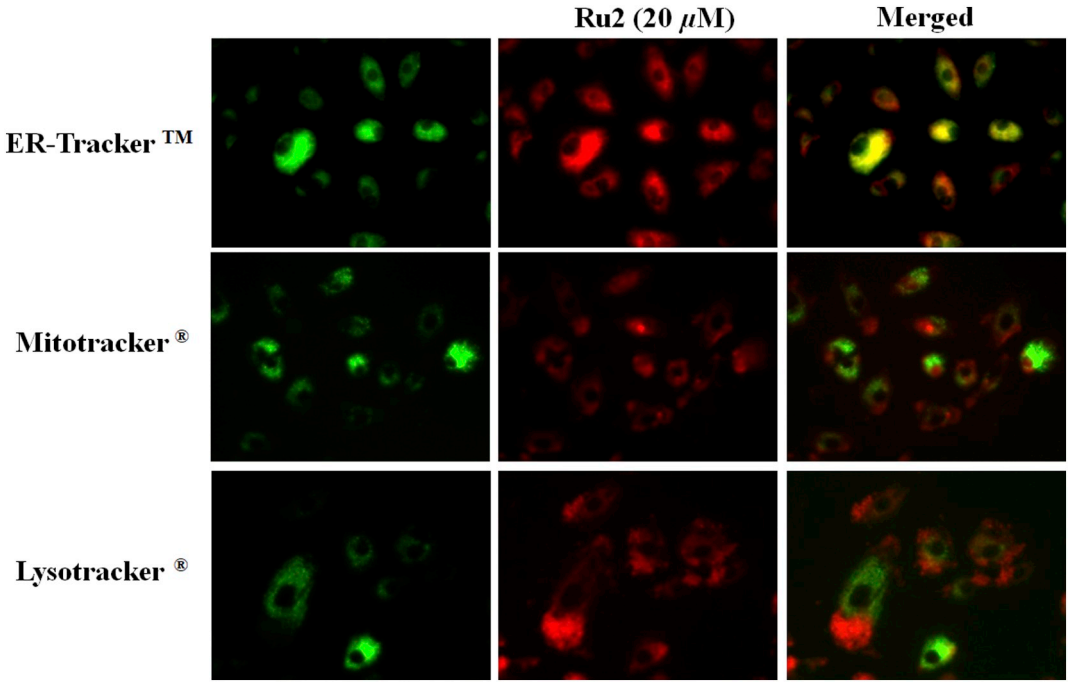

Fig. 1. Cell localization fluorescence microscopic imaging of **Ru2** with ER-Tracker™ (top), Mitotracker®(middle), and Lysotracker®(bottom). **Ru2** was excited at 460 nm. ER-Tracker™, Mitotracker® and Lysotracker® were excited at 546 nm.

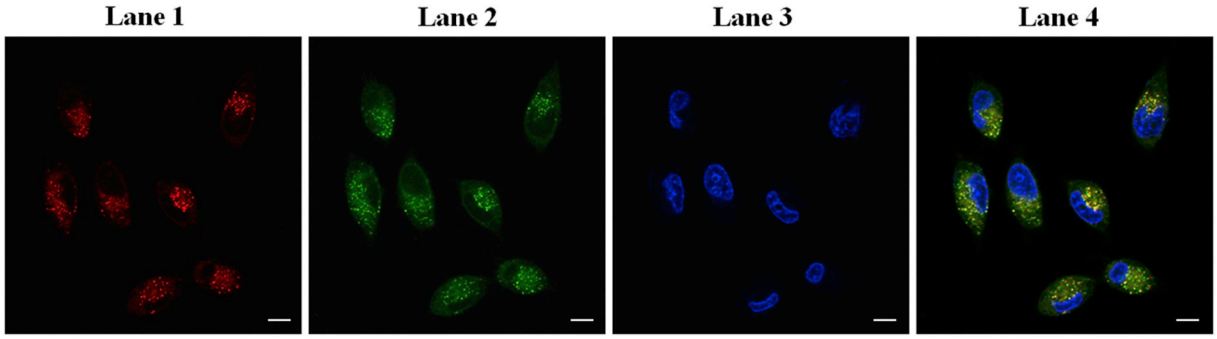

Fig. 2. Confocal fluorescence images of living HeLa cells incubated with 20 μM of **Ru2** in PBS (pH = 7.4) for 1 h at 37 °C, followed by 1 μM ER-Tracker™ and 5 μg mL^{-1} of DAPI, respectively. Lane 1, confocal fluorescence images of **Ru2**; lane 2, confocal fluorescence images of ER-Tracker™; lane 3, confocal fluorescence images of DAPI; lane 4, overlay of lane 1, lane 2 and lane 3.

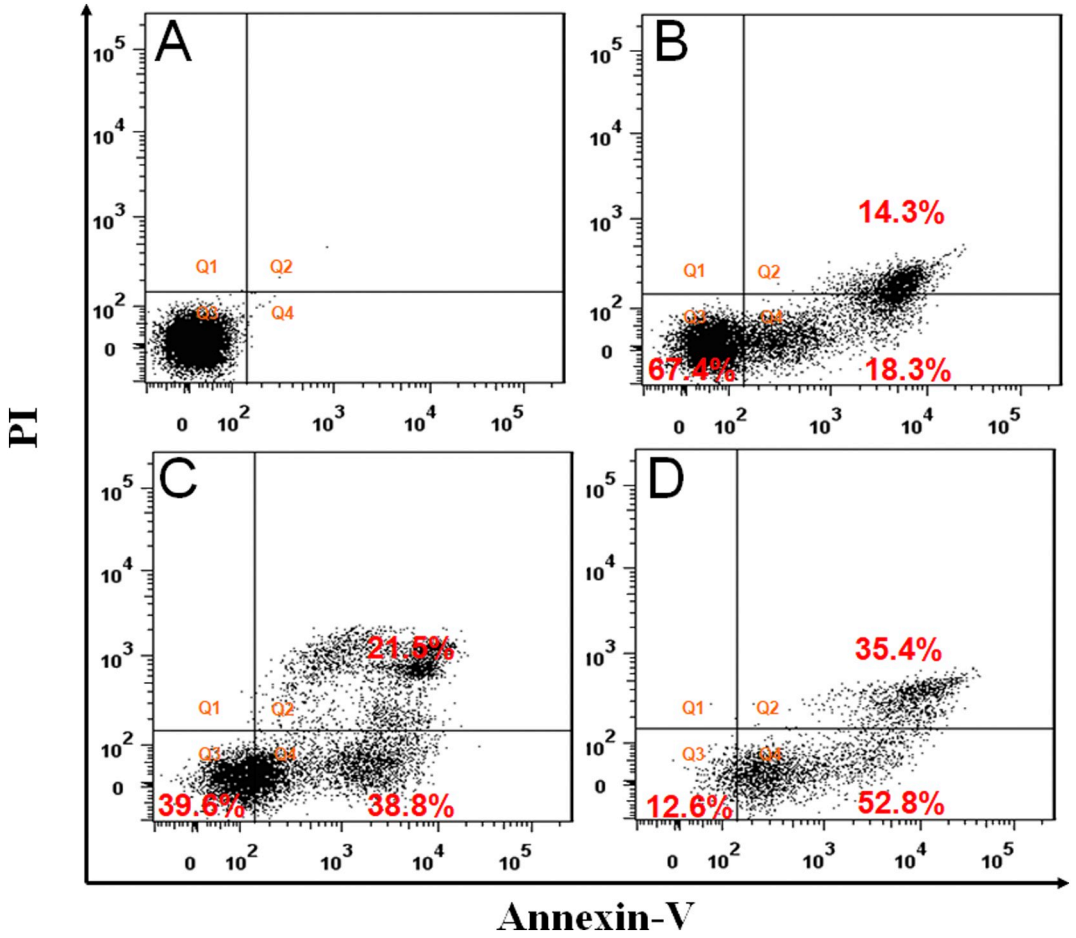

Fig. 3. Ru2 induced apoptotic cell death as examined by the annexinV-FITC/PI assay. HeLa cells were treated with different concentrations of **Ru2** for 24 h. (A) Control, (B) in the presence of **Ru2** (10 μM); (C) in the presence of **Ru2** (20 μM); (D) in the presence of **Ru2** (40 μM). The percentages of cells in each quadrant are shown (Q2: late apoptotic or necrotic cells, Q3: viable cells, Q4: early apoptotic cells).

0.92, suggesting that **Ru2** can selectively localize in the endoplasmic reticulum of living cells. These results indicated that the endoplasmic reticulum may be the primary target of **Ru2**. In addition, the ICP-MS experiments (Fig. S7) indicated that **Ru2** predominantly accumulated in the cytoplasm and only a small proportion entered the nuclei within 24 h. These results indicated that **Ru2** is not a nuclei-targeting Ru(II) complex. Because it showed the highest anticancer activity among the three complexes and accumulated primarily in the endoplasmic reticulum, **Ru2** was used to further study the underlying anticancer mechanisms.

3.4. Apoptosis assays

The externalization of phosphatidylserine (PS) on the outer surface of the cell membrane is a characteristic feature of cells entering apoptosis and can be detected by the binding of fluorescently labeled

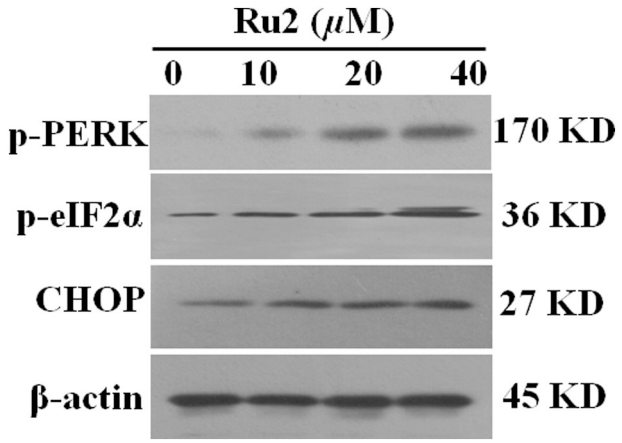

Fig. 4. Western blot analysis of ER-stress related proteins after treatment of HeLa cells with different concentrations of **Ru2**.

annexin V. Therefore, Alexa Fluor® 488 annexin V-PI double staining and FACS analysis were used to detect phosphatidylserine externalization [36,37]. As shown in Fig. 3, after 24 h of 10 μM **Ru2** treatment, 32.6% apoptotic cells could be detected, and with 20 μM **Ru2**, 38.8% and 21.5% of cells were found in early and late apoptotic stages, respectively. However, **Ru2** (40 μM) resulted in total apoptosis (early apoptotic + late apoptotic) in 88.2% of the cells. In comparison, the control cells remained 99% viable. The results showed that **Ru2** treatment of HeLa cells increased the number of early and late apoptotic cells in a dose-dependent manner, leading to cell death of the HeLa cells.

3.5. Western blot analysis

The stimulation of chemical drugs or the accumulation of misfolded proteins can cause ER stress and activate a signaling network, including apoptosis [38]. As **Ru2** could selectively accumulate in the ER, we assessed whether **Ru2** could induce ER stress. The early initiating events in ER stress is the phosphorylation of PKR-like ER kinase (PERK), which can activate eukaryotic initiation factor 2α (eIF2α). Next, phosphorylated eIF2α can induce the expression of enhancer binding protein homologous protein (CHOP), which has been described as a critical mediator of ER stress-induced apoptosis [39]. After treatment for 24 h with 10, 20 and 40 μM **Ru2**, which accumulated in the ER in a dose-dependent manner, the expression levels of phosphorylated PERK (p-PERK), eIF2α, and CHOP dramatically increased (Fig. 4), indicating that ER stress was induced.

To further determine the importance of CHOP induction in **Ru2**-induced cytotoxicity, the functionally validated SiRNA directed against CHOP was used. HeLa cells were transfected with the control SiRNA (SiCt) or CHOP SiRNA (SiCHOP) and treated with **Ru2** for 48 h with indicated concentrations. The SiRNA directed against CHOP significantly suppressed the expression of CHOP, while the control SiRNA had slight effect (Fig. 5A and Fig. S8). In addition, knockdown of CHOP resulted in significant attenuation of **Ru2**-induced cytotoxicity (Fig. 5B). These results indicate that **Ru2** exerts its toxicity through the endoplasmic reticulum stress/CHOP pathway, and CHOP is a key factor for **Ru2**-induced apoptosis.

Previuos studies have reported on caspase activation as one of the mechanisms of apoptotic process [40,41]. Therefore, we examined the effect of **Ru2** on caspase activation. HeLa cells were treated with **Ru2** in a concentration dependent manner and cleavage of caspase-7 and poly (ADP-ribose) polymerase (PARP) were detected by western blot analysis. As shown in Fig. S9, treatment with **Ru2** suppressed the expression of uncleaved caspase-7 (34 kDa) and increased the expression of cleaved caspase-7 (20 kDa) in a dose-dependent manner. Meanwhile, as an irreversible hallmark of apoptosis, the level of uncleaved PARP (116 kDa) was reduced, but the level of its active subunit (89 kDa) was increased after **Ru2** treatment, which indicates that HeLa cells have completed the apoptosis process. These present studies show that **Ru2** first induced ER stress, which led to apoptosis.

3.6. ROS study

In addition, intracellular ROS have been well documented to play a crucial role in apoptosis [42]. Therefore, we analyzed the **Ru2**-induced ROS generation by the ROS indicator DCFH-DA. DCFH-DA is oxidized by ROS to generate green fluorescent 2′,7′-dichlorofluorescein (DCF) [43]. Flow cytometry showed that **Ru2** increased the ROS levels in a dose-dependent manner (Fig. 6A). This clearly indicated that **Ru2** activated ROS generation and resulted in apoptotic cell death. To further examine the role of ROS generation in ruthenium (II)-induced cytotoxicity, we used H_2O_2 as a positive control and NAC as the ROS scavenger. The results showed that pretreatment of the cells with NAC decreased both H_2O_2 and **Ru2**-induced ROS generation, respectively (Fig. 6B). In addition, the presence of NAC attenuated H_2O_2-induced cytotoxicity and the cytotoxicity of **Ru2** toward HeLa cells (Fig. 6C). Taken together, these results indicate that **Ru2** can induce ROS, and ROS plays roles in **Ru2**-induced apoptosis.

3.7. Induction of mitochondrial dysfunction

ROS generation is known to result in mitochondrial membrane depolarization and to cause mitochondrial dysfunction. Hence, we further evaluated whether **Ru2** induced mitochondrial dysfunction by measuring the mitochondrial membrane potential using the lipophilic cationic molecular probe JC-1. JC-1 exhibits mitochondrial membrane potential-dependent, indicated by a fluorescence emission shift from J-aggregates with red fluorescence (~590 nm) to J-monomers with green fluorescence (~529 nm) in accordance with the loss of mitochondrial membrane potential. As shown in Fig. 7, JC-1 showed red fluorescence

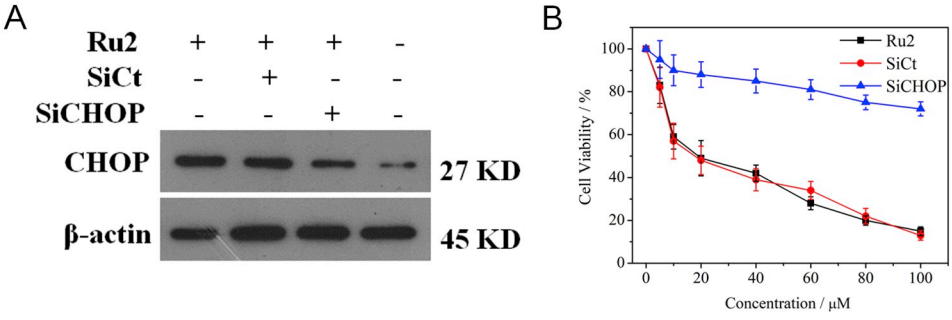

Fig. 5. CHOP was essential for **Ru2**-induced cytotoxicity. (A) After transfected with control siRNAs or CHOP siRNAs, siRNAs transfected HeLa cells were treated with **Ru2** for 48 h. CHOP expression was detected by western blot. (B) Effects of siRNAs on **Ru2**-induced cytotoxicity. HeLa cells were exposed to siRNAs or CHOP siRNAs then treated with **Ru2** for 48 h with indicated concentrations. Cell viability was assessed by MTT assay.

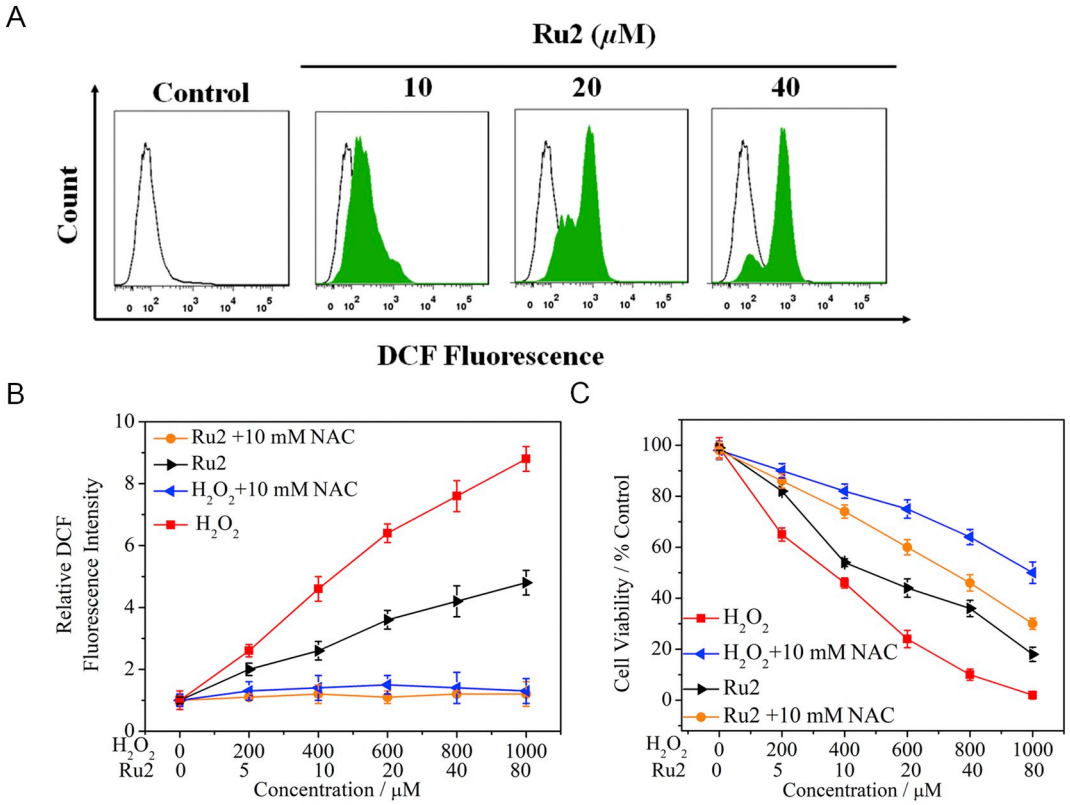

Fig. 6. (A) DCFH-DA detection of ROS levels in HeLa cells treated with **Ru2** at 10, 20 and 40 μM for 12 h using flow cytometric analysis. (B) The ROS level was expressed as the relative fluorescence intensity after 12 h of treatment with **Ru2** and H_2O_2 with or without NAC at the indicated concentrations. (C) Effects of NAC (10 mM) on **Ru2** or H_2O_2-induced cytotoxicity. HeLa cells were exposed to different doses of **Ru2** or H_2O_2 with or without NAC for 12 h. Cell viability was assessed by MTT assay. DCF 2′,7′-dichlorofluorescein.

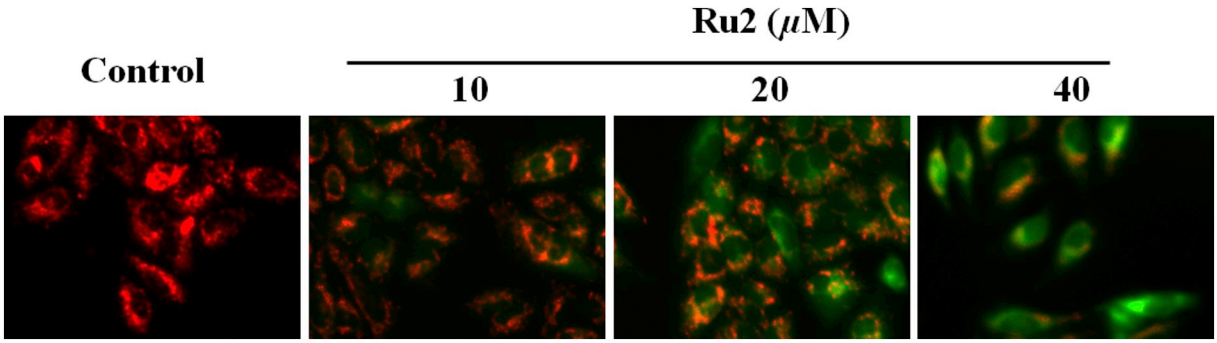

Fig. 7. Fluorescence images of the JC-1 labeled HeLa cells treated with 10, 20 and 40 μM **Ru2** for 12 h was observed on a fluorescence microscope to monitor changes in the mitochondrial membrane potential.

(JC-1 aggregates) in the control. In contrast, **Ru2** (10, 20 and 40 μM) treatments caused a significantly shift in the color of JC-1 fluorescence from red to green, indicating the induction of mitochondrial membrane depolarization and mitochondrial dysfunction. Thus, **Ru2** selectively targets the ER and induces apoptosis by two pathways: ER stress and mitochondrial dysfunction (Fig. 8).

4. Conclusions

Three new Ru(II) complexes containing a *p*-cresol group were synthesized and characterized. An *in vitro* cytotoxicity assay indicated that these ruthenium (II) complexes exhibited potent cancer inhibitory effects against selected cancer cell lines. Interestingly, **Ru2** showed higher anticancer activity than **Ru1** and **Ru3**. Subcellular distribution studies showed that **Ru2** localized preferentially in the endoplasmic reticulum. The results of the western blot analysis demonstrated that CHOP was activated in **Ru2**-treated HeLa cell. The silencing of CHOP by RNA interference significantly reduced the cytotoxicity of **Ru2**. Additionally, **Ru2** increased the intracellular ROS levels and reduced the mitochondrial membrane potential in a concentration-dependent manner. Thus, **Ru2** induced apoptosis through endoplasmic reticulum stress and ROS-mediated mitochondria dysfunction pathways, indicating that **Ru2** could be a strong candidate for therapeutic application in human cancers.

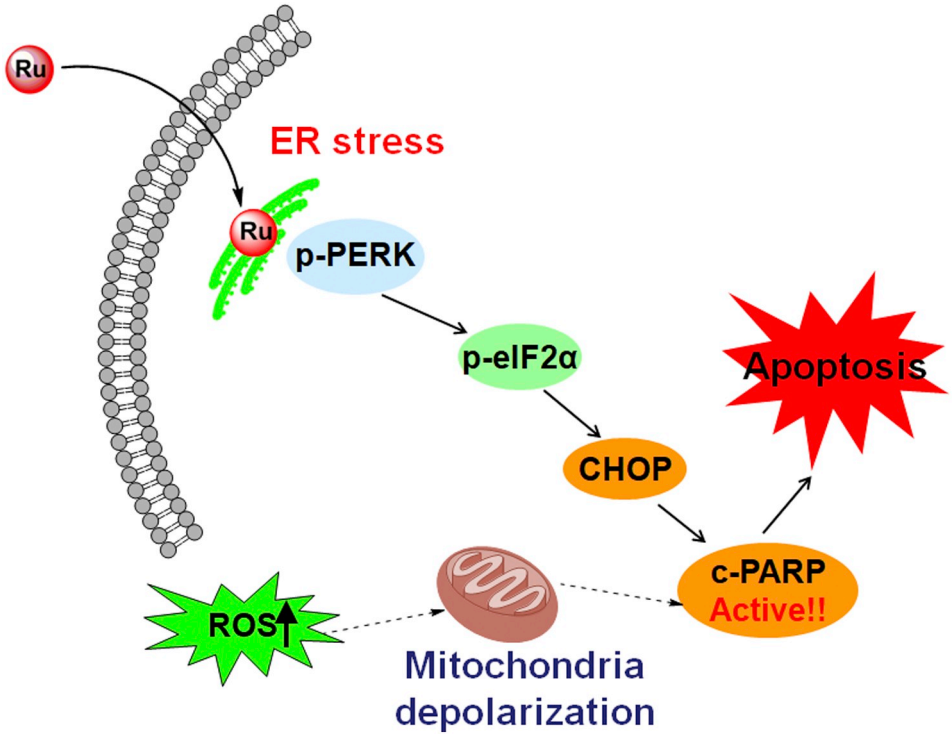

Fig. 8. Proposed anticancer pathway by **Ru2**.

Acknowledgements

This work was supported by the National Science Foundation of China (No. 21301034, 21771042) and the National Science Foundation of Guangdong Province (No. S2013040014083, 2016A030310298).

Appendix A. Supplementary data

Supplementary data to this article can be found online at https://doi.org/10.1016/j.jinorgbio.2018.11.015.

References

[1] L.L. Zeng, P. Gupta, Y.L. Chen, E.J. Wang, L.N. Ji, H. Chao, Z.S. Chen, The development of anticancer ruthenium(II) complexes: from single molecule compounds to nanomaterials, Chem. Soc. Rev. 46 (2017) 5771–5804.
[2] A. Bergamo, G. Sava, Ruthenium complexes can target determinants of tumour malignancy, Dalton Trans. (2007) 1267–1272.
[3] C.G. Hartinger, M.A. Jakupec, S. Zorbas-Seifried, M. Groessl, A. Egger, W. Berger, H. Zorbas, P.J. Dyson, B.K. Keppler, KP1019, a new redox-active anticancer agent-preclinical development and results of a clinical phase I study in tumor patients, Chem. Biodivers. 5 (2008) 2140–2155.
[4] F.P. Rodrigues, Z.A. Carneiro, P. Mascharak, C. Curti, R.S. da Silva, Incorporation of a ruthenium nitrosyl complex into liposomes, the nitric oxide released from these liposomes and HepG2 cell death mechanism, Coord. Chem. Rev. 306 (2016) 701–707.
[5] W.L. Kwong, K.Y. Lam, C.N. Lok, Y.T. Lai, P.Y. Lee, C.M. Che, A macrocyclic ruthenium(III) complex inhibits angiogenesis with down-regulation of vascular endothelial growth factor receptor-2 and suppresses tumor growth in vivo, Angew. Chem. 128 (2016) 13722–13726.
[6] M. Montani, G.V.B. Pazmay, A. Hysi, G. Lupidi, R. Pettinari, V. Gambini, M. Tilio, F. Marchetti, C. Pettinari, S. Ferraro, The water soluble ruthenium(II) organometallic compound [Ru(p-cymene)(bis(3,5 dimethylpyrazol-1-yl)methane)Cl]Cl suppresses triple negative breast cancer growth by inhibiting tumor infiltration of regulatory T cells, Pharmacol. Res. 107 (2016) 282–290.
[7] G.Y. Li, T. Sasaki, S.S. Asahina, M.C. Roy, T. Mochizuki, K. Koizumi, Y. Zhang, Patching of lipid rafts by molecular self-assembled nanofibrils suppresses Cancer cell migration, Chem 2 (2017) 283–298.
[8] M.R. Gill, S.N. Harun, S. Halder, R.A. Boghozian, K. Ramadan, H. Ahmad, K.A. Vallis, A ruthenium polypyridyl intercalator stalls DNA replication forks, radiosensitizes human cancer cells and is enhanced by Chk1 inhibition, Sci. Rep. 6 (2016) 31973.
[9] M.V. Babak, S.M. Meier, K.V.M. Huber, J. Reynisson, A.A. Legin, M.A. Jakupec, A. Roller, A. Stukalov, M. Gridling, K.L. Bennett, J. Colinge, W. Berger, P.J. Dyson, G. Superti-Furga, B.K. Keppler, C.G. Hartinger, Target profiling of an antimetastatic RAPTA agent by chemical proteomics: relevance to the mode of action, Chem. Sci. 6 (2015) 2449–2456.
[10] L. Feng, Y. Geisselbrecht, S. Blanck, A. Wilbuer, G.E. Atilla-Gokcumen, P. Filippakopoulos, K. Kräling, M.A. Celik, K. Harms, J. Maksimoska, Structurally sophisticated octahedral metal complexes as highly selective protein kinase inhibitors, J. Am. Chem. Soc. 133 (2011) 5976–5986.
[11] C. Tan, S. Lai, S. Wu, S. Hu, L. Zhou, Y. Chen, M. Wang, Y. Zhu, W. Lian, W. Peng, Nuclear permeable ruthenium(II) β-carboline complexes induce autophagy to antagonize mitochondrial-mediated apoptosis, J. Med. Chem. 53 (2010) 7613–7624.
[12] V. Pierroz, T. Joshi, A. Leonidova, C. Mari, J. Schur, I. Ott, L. Spiccia, S. Ferrari, G. Gasser, Molecular and cellular characterization of the biological effects of ruthenium(II) complexes incorporating 2-pyridyl-2-pyrimidine-4-carboxylic acid, J. Am. Chem. Soc. 134 (2012) 20376–20387.
[13] X.J. Meng, M.L. Leyva, M. Jenny, I. Gross, S. Benosman, B. Fricker, S. Harlepp, P. Hébraud, A. Boos, P. Wlosik, P. Bischoff, C. Sirlin, M. Pfeffer, J.P. Loeffler, C. Gaiddon, A ruthenium-containing organometallic compound reduces tumor growth through induction of the endoplasmic reticulum stress gene CHOP, Cancer Res. 69 (13) (2009) 5458–5466.
[14] M.R. Gill, D. Cecchin, M.G. Walker, R.S. Mulla, G. Battaglia, C. Smythe, J.A. Thomas, Targeting the endoplasmic reticulum with a membrane interactive luminescent ruthenium(II) polypyridyl complex, Chem. Sci. 4 (2013) 4512–4519.
[15] J.S. Nam, M.G. Kang, J. Kang, S.Y. Park, S.J.C. Lee, H.T. Kim, J.K. Seo, O.H. Kwon, M.H. Lim, H.W. Rhee, Endoplasmic reticulum-localized iridium(III) complexes as efficient photodynamic therapy agents via protein modifications, J. Am. Chem. Soc. 138 (2016) 10968–10977.
[16] R. Cao, J.L. Jia, X.C. Ma, M. Zhou, H. Fei, Membrane localized iridium(III) complex induces endoplasmic reticulum stress and mitochondria-mediated apoptosis in human cancer cells, J. Med. Chem. 56 (2013) 3636–3644.
[17] S. Mandal, D.K. Poria, R. Ghosh, P.S. Ray, P. Gupta, Development of a cyclometalated iridium complex with specific intramolecular hydrogen-bonding that acts as a fluorescent marker for the endoplasmic reticulum and causes photoinduced cell death, Dalton Trans. 43 (2014) 17463–17474.
[18] T.T. Zou, C.N. Lok, Y.M.E. Fung, C.M. Che, Luminescent organoplatinum(II) complexes containing bis(N-heterocyclic carbene) ligands selectively target the endoplasmic reticulum and induce potentphoto-toxicity, Chem. Commun. 49 (2013) 5423–5425.
[19] Y. Xu, H.M. Yu, H.J. Qin, J.S. Kang, C.Y. Yu, J.T. Zhong, J. Su, H.Y. Li, L.K. Sun, Inhibition of autophagy enhances cisplatin cytotoxicity through endoplasmic reticulum stress in human cervical cancer cells, Cancer Lett. 314 (2012) 232–243.
[20] W.L. Kwong, R.W.Y. Sun, C.N. Lok, F.M. Siu, S.Y. Wong, K.H. Low, C.M. Che, An ytterbium(III) porphyrin induces endoplasmic reticulum stress and apoptosis in cancer cells: cytotoxicity and transcriptomics studies, Chem. Sci. 4 (2013) 747–754.
[21] C.Y. Liu, R.J. Kaufman, The unfolded protein response, J. Cell Sci. 116 (2003) 1861–1862.
[22] M.J. Berridge, The endoplasmic reticulum: a multifunctional signaling organelle, Cell Calcium 32 (2002) 235–249.
[23] Y. Liu, Y. Ye, Proteostasis regulation at the endoplasmic reticulum: a new

perturbation site for targeted cancer therapy, Cell Res. 21 (2011) 867–883.
[24] M. Kurtoglu, K. Philips, H. Liu, L.H. Boise, T.J. Lampidis, High endoplasmic reticulum activity renders multiple myeloma cells hypersensitive to mitochondrial inhibitors, Cancer Chemother. Pharmacol. 66 (2010) 129–140.
[25] S.J. Healy, A.M. Gorman, P. Mousavi-Shafaei, S. Gupta, A. Samali, Targeting the endoplasmic reticulum-stress response as an anticancer strategy, Eur. J. Pharmacol. 625 (2009) 234–246.
[26] L. Li, Y.S. Wong, T.F. Chen, C. Fan, W. Zheng, Ruthenium complexes containing bisbenzimidazole derivatives as a new class of apoptosis inducers, Dalton Trans. 41 (2012) 1138–1141.
[27] C. Qian, J.Q. Wang, C.L. Song, L.L. Wang, L.N. Ji, H. Chao, The induction of mitochondria-mediated apoptosis in cancer cells by ruthenium(II) asymmetric complexes, Metallomics 5 (2013) 844–854.
[28] C.P. Tan, S.H. Wu, M. Wang, Y. Chen, L. Zhou, Y. Zhu, W. Lian, W. Peng, L. Ji, A.L. Xu, Synthesis, structures, cellular uptake and apoptosis-inducing properties of highly cytotoxic ruthenium-Norharman complexes, Dalton Trans. 40 (2011) 8611–8621.
[29] C. Xia, Q. Meng, L.Z. Liu, Y. Rojanasakul, X.R. Wang, B.H. Jiang, Reactive oxygen species regulate angiogenesis and tumor growth through vascular endothelial growth factor, Cancer Res. 67 (2007) 10823–10830.
[30] T. Ozben, Oxidative stress and apoptosis: impact on cancer therapy, J. Pharm. Sci. 96 (2007) 2181–2196.
[31] M. Yamada, Y. Tanaka, Y. Yoshimoto, S. Kuroda, I. Shimao, Synthesis and properties of diamino-substituted dipyrido[3,2-*a*: 2′,3′-*c*]phenazine, Bull. Chem. Soc. Jpn. 65 (1992) 1006–1011.
[32] B.P. Sullivan, D.J. Salmon, T.J. Meyer, Mixed phosphine 2,2′-bipyridine complexes of ruthenium, Inorg. Chem. 17 (1978) 3334–3341.
[33] T.J. Mosmann, Rapid colorimetric assay for cellular growth and survival: application to proliferation and cytotoxicity assays, J. Immunol. Methods 65 (1983) 55–63.
[34] K.W. Mudasir, N. Yoshioka, H. Inoue, DNA binding of iron(II) complexes with 1,10-phenanthroline and 4,7-diphenyl-1,10-phenanthroline: salt effect, ligand substituent effect, base pair specificity and binding strength, J. Inorg. Biochem. 94 (2003) 263–271.
[35] H.J. Yu, Y. Chen, L. Yu, Z.F. Hao, L.H. Zhou, Synthesis, visible light photocleavage, antiproliferative and cellular uptake properties of ruthenium complex [Ru(phen)$_2$(mitatp)]$^{2+}$, Eur. J. Med. Chem. 55 (2012) 146–154.
[36] I. Vermes, C. Haanen, H. Steffens-Nakken, C. Reutelingsperger, A novel assay for apoptosis flow cytometric detection of phosphatidylserine expression on early apoptotic cells using fluorescein labelled annexin V, J. Immunol. Methods 184 (1995) 39–51.
[37] R.N. Bhattacharjee, K.S. Park, Y. Kumagai, K. Okada, M. Yamamoto, S. Uematsu, K. Matsui, H. Kumar, T. Kawai, T. Iida, T. Honda, O. Takeuchi, S. Akira, VP1686, a Vibrio type III secretion protein, induces toll-like receptor-independent apoptosis in macrophage through NF-κB inhibition, J. Biol. Chem. 281 (2006) 36897–36904.
[38] I. Kim, W. Xu, J.C. Reed, Cell death and endoplasmic reticulum stress: disease relevance and therapeutic opportunities, Nat. Rev. Drug Discov. 7 (2008) 1013–1030.
[39] A. Gorlach, P. Klappa, T. Kietzmann, The endoplasmic reticulum: folding, calcium homeostasis, signaling, and redox control, Antioxid. Redox Signal. 8 (2006) 1391–1418.
[40] D.G. Breckenridge, M. Germain, J.P. Mathai, M. Nguyen, G.C. Shore, Regulation of apoptosis by endoplasmic reticulum pathways, Oncogene 22 (2003) 8608–8618.
[41] R.J. Youle, A. Strasser, The BCL-2 protein family: opposing activities that mediatecell death, Nat. Rev. Mol. Cell Biol. 9 (2008) 47–59.
[42] T. Ozben, Oxidative stress and apoptosis: impact on cancer therapy, J. Pharm. Sci. 96 (2007) 2181–2196.
[43] L.R. Silveira, L. Pereira-Da-Silva, C. Juel, Y. Hellsten, Formation of hydrogen peroxide and nitric oxide in rat skeletal muscle cells during contractions, Free Radic. Biol. Med. 35 (2003) 455–464.